

# The nature of strings in the nebula around $\eta$ Carinae<sup>★</sup>

K. Weis<sup>1,2,★★</sup>, W.J. Duschl<sup>1,3</sup>, and Y.-H. Chu<sup>2,★★</sup>

<sup>1</sup> Institut für Theoretische Astrophysik, Tiergartenstrasse 15, D-69121 Heidelberg, Germany

<sup>2</sup> University of Illinois, Department of Astronomy, 1002 W. Green Street, Urbana, IL 61801, USA

<sup>3</sup> Max-Planck-Institut für Radioastronomie, Auf dem Hügel 69, D-53121 Bonn, Germany

Received 6 October 1998 / Accepted 5 July 1999

**Abstract.**  $\eta$  Carinae is one of the most extreme cases of a Luminous Blue Variable star. A bipolar nebula of  $17''$  size surrounds the central object. Even further out, a large amount of filamentary material extends to a distance of  $30''$  or about 0.3 pc. In this paper we present a detailed kinematic and morphological analysis of some outer filaments in this nebula which we call *strings*. All strings are extremely long and narrow structures. We identified 5 strings which have sizes of 0.058 to 0.177 pc in length and a width of only 0.002 pc. Using high-resolution long-slit echelle spectroscopy it was found that the strings follow a Hubble law with velocities increasing towards larger distances from the star. With these unique properties, *high collimation* and *linear increase* of the radial velocity the strings represent a newly found phenomena in the structure and evolution of nebulae around LBVs. Finally, we show that morphologically similar strings can be found in the planetary nebula NGC 6543, a possible PN-counterpart to this phenomenon.

**Key words:** stars: individual:  $\eta$  Car – stars: evolution – stars: mass-loss – ISM: bubbles – ISM: jets and outflows

## 1. Introduction

At a present day mass of  $M \sim 120 M_{\odot}$  and a luminosity of  $L \sim 10^{6.7} L_{\odot}$  (Humphreys & Davidson 1994, Davidson & Humphreys 1997)  $\eta$  Carinae tops the Hertzsprung-Russell Diagram (HRD) and is certainly among the most massive stars observed as yet. Even if the recently re-discussed binary hypothesis for  $\eta$  Car (Damineli 1996, Damineli et al. 1997, Davidson 1997) should turn out to apply, at least one component

has to have a mass exceeding  $\sim 60 M_{\odot}$ , which again puts it into the realm of the most massive stars.  $\eta$  Car is a member of the stellar class of *Luminous Blue Variables* (LBVs), which start as main-sequence O stars with masses  $M_{ZAMS} \geq 50 M_{\odot}$ ; these stars evolve towards cooler temperatures at the end of hydrogen-core burning and may enter an unstable phase at an age of roughly  $3 \cdot 10^6$  years (Langer et al. 1994). This so-called LBV phase starts when the stars reach the Humphreys-Davidson limit (Humphreys & Davidson 1979, 1994) in the HRD. Analyzing HRDs of the Galaxy and the LMC, Humphreys (1978, 1979) and Humphreys & Davidson (1979) found a lack of very luminous red supergiants. Obviously the most massive stars do not evolve into red supergiants but instead their evolution is reversed towards the blue supergiant part in the HRD when they approach the Humphreys-Davidson limit as LBVs.

One of the most prominent characteristics of the unstable LBV phase is a very high mass loss rate (characteristically about several  $10^{-4} M_{\odot} \text{ yr}^{-1}$  with values even higher during giant eruptions). Strong stellar winds and giant eruptions peel off parts of the stellar envelope and form small circumstellar nebulae around LBVs, so-called LBV nebulae (LBVN; Nota et al. 1995). In the same manner  $\eta$  Car formed its nebula in a quite dramatic way. Having been a  $\sim 6^{\text{m}}$  star for a long time (with only small changes)  $\eta$  Car drastically brightened around 1843 AD (Herschel 1847, Innes 1903, van Genderen & Thé 1984, Viotti 1995) and became a  $\sim -1^{\text{m}}$  star for about 5 years. This giant eruption led to the formation of a nebula that was found only a century later. Nearly simultaneously Gaviola (1946, 1950) and Thackeray (1949, 1950) photographed the nebula for the first time. Because of its odd man-like shape Gaviola named it the *Homunculus*. Later it became clear that the Homunculus is only the brightest region of a larger bipolar nebula, consisting of two lobes of  $\sim 8 \dots 9''$  diameter each. They are separated by an equatorial plane structure (Duschl et al. 1995). The high resolution Hubble Space Telescope (HST, Morse et al. 1998) images support this model, showing clearly the bipolarity of the Homunculus. The deepest HST pictures (200 s in the F656N and F658N filters) reveal an even larger nebula consisting of a variety of filamentary structures like knots, arcs and strings at a distance of up to  $30''$  from  $\eta$  Car. The sizes of filaments vary in a wide range from fractions of an arcsecond to several arcseconds.

Send offprint requests to: K. Weis, Heidelberg, Germany  
(kweis@ita.uni-heidelberg.de)

\* Based on observations with the NASA/ESA Hubble Space Telescope, obtained at the Space Telescope Science Institute, which is operated by the Association of Universities for Research in Astronomy, Inc. under NASA contract No. NAS5-26555.

\*\* Visiting Astronomer, Cerro Tololo Inter-American Observatory, National Optical Astronomy Observatories, operated by the Association of Universities for Research in Astronomy, Inc., under contract with the National Science Foundation.

Correspondence to: K. Weis, Heidelberg, Germany

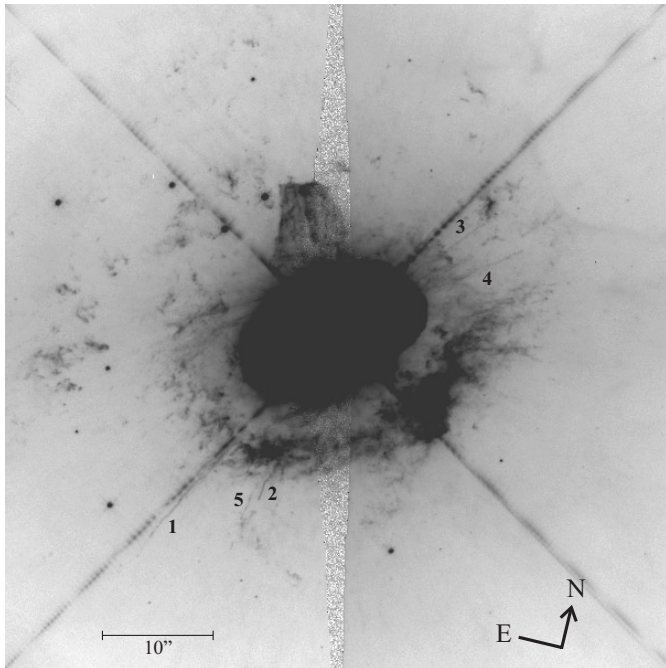


**Fig. 1.** HST picture of the nebula around  $\eta$  Car composed of frames of different exposure times in the F656N filter. The field of view (FOV) is  $60'' \times 60''$ . The five morphologically identified strings are indicated. North and east markers in the plot indicate the orientation of the image.

Analysis of the kinematics of the Homunculus and the filaments has contributed considerably to the understanding of the structure and nature of the nebula. Radial velocity (Meaburn et al. 1987, 1993, 1996, Hillier & Allen 1992) and proper motion (Walborn 1976, Walborn et al. 1978, Walborn & Blanco 1988, Currie et al. 1996, Smith & Gehrz 1998) measurements revealed velocities up to  $10^3 \text{ km s}^{-1}$ .

A comprehensive study of the full outer filamentary nebula of  $\eta$  Car will be found in Weis & Duschl (1999, in prep.). In the present paper we concentrate on several very narrow, long and coherent structures which we will refer to as *strings*. As yet, we investigated in detail the morphology of the 5 most prominent strings. Moreover, we show additional kinematic analysis of 3 of these strings, including a full velocity coverage of the longest string. With the high-resolution images of the HST it was possible for the first time to study the LBVN of  $\eta$  Car in such a detail that structures as narrow as the strings could be resolved and analyzed. This paper describes the morphology of the strings and presents their kinematic properties. We also discuss possible formation mechanism of the strings and address their uniqueness.

## 2. Observation and data reduction

### 2.1. Imaging

All strings were first detected in the high-resolution images of the Homunculus nebula made with the HST, as yet the only telescope able to resolve such small scale structures (width:  $0''.2$ – $0''.4$  or  $\sim 10^{-2}$  pc). All HST images we used were taken from the

Canadian Astrophysics Data Center (CADC) archive and were recalibrated using their optimal calibration data. We retrieved all frames obtained in the F656N ( $H_\alpha$ ) and F658N ( $[\text{N II}]$ ) filters<sup>1</sup>. The strings were not visible in any other filters. In each filter the observations were carried out with three different exposure times, 0.011, 4 and 200 s. For reduction, combination of the images and cosmic-ray cleaning we followed the standard procedures recommended for WFPC2 data. Frames of the same filter were combined weighting and scaling with the exposure time and used to correct the bleeding by substituting the pixels with bleeding by pixels from frames with a lower exposure time. Since most of the features seen in the nebula around  $\eta$  Carinae have expansion velocities of several  $\times 10^2 \text{ km s}^{-1}$  (Meaburn et al. 1987, 1996, Hillier & Allen 1992, Weis et al. in prep., and this paper) many of the features seen in the F656N filter are contaminated by blueshifted  $[\text{N II}]$ -emission at  $6583 \text{ \AA}$  and emission seen in the F658N filter originates in redshifted emission from the  $H_\alpha$  line. Due to the Doppler shifts, the two filters are no longer genuine  $H_\alpha$  and  $[\text{N II}]$  filters for the expanding material of  $\eta$  Car. This effect is also responsible for the wavelength-dependent length of string 1, which is longer in the F656N than in the F658N image. While we only show images of the F656N filter in the paper we always compare the measured sizes in both narrow band images, keeping the Doppler shifts in mind. Fig. 1 shows a  $60'' \times 60''$  section of the final F656N WFPC2 frame. A north-east vector indicates the celestial directions. We restrained from rotating the images because of the loss of resolution when using the IRAF rotation task. All images therefore have the original HST sampling of  $0''.0455 \text{ pixel}^{-1}$  for the PC and  $0''.0996 \text{ pixel}^{-1}$  for the WFC.

### 2.2. Long-slit echelle spectroscopy

To obtain kinematic information on the strings we used the echelle spectrograph on the 4 m telescope at the Cerro Tololo Inter-American Observatory. We observed in the long-slit mode, inserting a post-slit  $H_\alpha$  filter ( $6563/75 \text{ \AA}$ ) and replaced the cross-disperser with a flat mirror. The  $791 \text{ mm}^{-1}$  echelle grating was used, where the slit-width was  $250 \mu\text{m}$  ( $= 1''.64$ ) resulting in an instrumental FWHM at the  $H_\alpha$  line of about  $14 \text{ km s}^{-1}$ .

Data were recorded with the long focus red camera and the  $2048 \times 2048$  Tek2K4 CCD was used. The pixel size was  $0.08 \text{ \AA pixel}^{-1}$  along the dispersion, and  $0''.26 \text{ pixel}^{-1}$  on the spatial axis. Due to vignetting, the slit length was limited to  $\sim 4'$ . Seeing was  $\sim 2''$  during the observations and the weather was not photometric. Thorium-Argon comparison lamp frames were taken for wavelength calibration and geometric distortion correction. The slit positions were referenced with respect to Thé et al.'s (1980) star #66 in the Trumpler 16 cluster.

Five positions were observed covering three of the five visually identified strings. The spectra were taken  $30''$ ,  $32''$ ,  $34''$ ,

<sup>1</sup> F656N – program number: 5239; P.I.: J.A. Westphal; dataset names: U2DH0101T ... U2DH0106T; F658N – program number: 5188; P.I.: W. Sparks; dataset names: U2410501T, U2410502P ... U2410506P

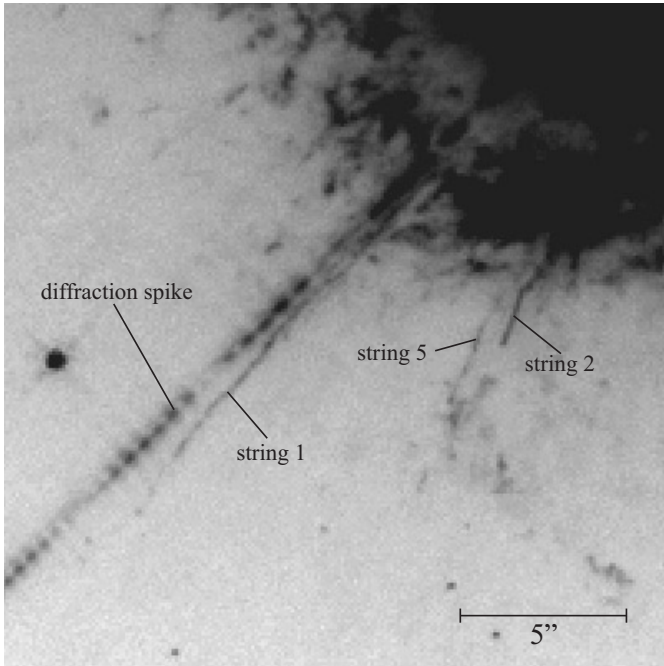


**Fig. 2.** Blow up of the HST picture of the nebula around  $\eta$  Car for a more detailed presentation of strings 1 (long string to the left), 2 (shortest to the right) and 5 (very faint in the middle).

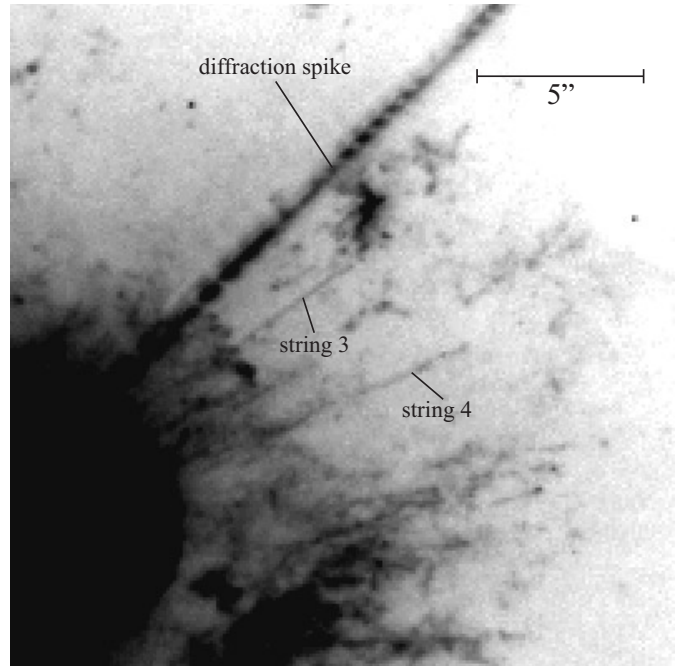


**Fig. 3.** Blow up of the HST picture of the nebula around  $\eta$  Car for a more detailed view of strings 3 (upper) and 4 (lower).

36'', and 38'' south of our reference star (Slits 30S, 32S, 34S, 36S, and 38S, respectively). The slit was rotated to a position angle of  $PA = 132^\circ$  to align it with the major axis of the Homunculus nebula and the general direction of the strings. Figs. 5 show the spectra at the five positions, the strings are marked. The exposure time was 30 s for slit 30S, 90 s for slit 32S and 180 s for the slits 34S, 36S and 38S.

### 3. Identification and morphology of the strings

A large number of filamentary structures can be identified in the deep HST picture of the Homunculus nebula around  $\eta$  Car. Among all these morphologically different structures a few long, coherent and very narrow features are the most amazing objects we found. These features are the above introduced *strings*. We identified 5 such strings by visual inspection. On smaller length scales, morphologically similar features can be seen (Weis & Duschl 1999 in prep.). However, due to confusion with background emission in the spectra, a detailed analysis was not possible in the work presented here. Of those 5 strings 3 were found in the south-eastern, and 2 in the north-western part of the nebula. None were detected in the other two quadrants. The strings are marked and named in Fig. 1. A blowup of the HST image in Fig. 2 gives a closer view of strings 1, 2 and 5 while Fig. 3 shows string 3 and 4 in more detail.

The observed lengths of the strings range between  $4''.0$  and  $15''.9$ . Towards the center of  $\eta$  Car we cannot distinguish the strings from the overall emission of other knots and filaments. At the very end of the strings the surface brightness decreases, and the strings might extend further at a level below the detection

limit. Therefore, the far end of the strings is not well determined, and all measured lengths are only lower limits.

To determine the lengths of the strings we adopt a distance of 2.3 kpc to  $\eta$  Car (Walborn 1995, Davidson & Humphreys 1997). However, the distance to the Carina H II region still has not been accurately determined because of the strong and variable reddening in this region. In the following, all sizes are measured as a width at the base rather than FWHM.

*String 1* lies in the south-eastern part of the nebula (see Figs. 1 and 2) and is the longest of all detected. The total measured length is  $15''.86 = 0.177 \text{ pc} \sim 36\,500 \text{ AU}$ . This length is comparable to the combined size of the two lobes of the central bipolar nebula.

We used the PC F658N images to determine the width of string 1. In this image the inner part (closer to  $\eta$  Car) of the string was resolved. The images show a width of about 5 pixels, corresponding to  $0''.23 = 0.003 \text{ pc} \sim 500 \text{ AU}$ . The resolution of the WFC is insufficient; at 2 pixels the strings cannot be reliably resolved, but the WFC image suggests that the width does not change significantly along the string. This leads to a length-to-width ratio of  $\sim 70$ .

If the string extends all the way to the star, an assumption supported by the orientation of the string with respect to  $\eta$  Car, the total projected length of the string is  $29''.0 = 0.323 \text{ pc} \sim 66\,700 \text{ AU}$  and the length-to-width ratio would be 128. However, in the following, when not stated explicitly otherwise, we always give the observed rather than the extrapolated length-to-width ratio, i.e., a lower limit for this quantity.

Even though string 1 seems very straight, small, almost periodic wiggles occur at a scale of several arcseconds as one can see in Fig. 2. At its inner end, string 1 seems either to have a split

**Table 1.** Properties of the strings

string	observed length [pc]	$v_{\min}$ [km s $^{-1}$ ]	$v_{\max}$ [km s $^{-1}$ ]	[N II] $\lambda$ 6583/H $\alpha$
1	0.177	-522	-995	3.3
2	0.044	-442	-591	2.7
3	0.095	-	-	-
4	0.103	-	-	-
5	0.058	-383	-565	3.0

of a length of  $\sim 1''.5$  or to be projected onto another string-like feature in the fore- or background. The intensity varies along the string and decreases rapidly at its outer end. No periodic or symmetric variations were found. Note that String 1 corresponds to the structure called *jet* and *spike* by Meaburn et al. (1987) and Meaburn et al. (1996), respectively.

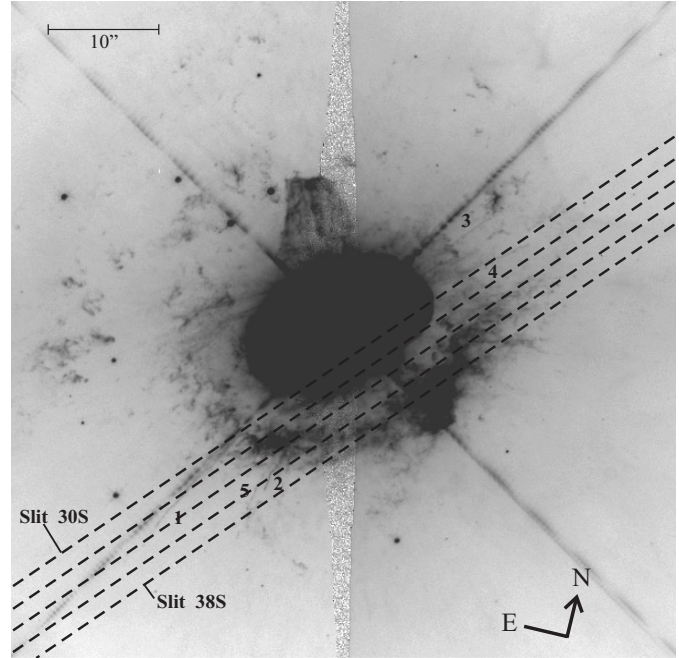
*String 2* is shorter than String 1 and has a higher surface brightness. It lies close to String 1 in the south-eastern part of the nebula. String 2 is  $4''.0$  long ( $= 0.044$  pc  $\sim 9$  000 AU). The width was determined in the same way as for string 1. A total width of  $0''.13$  ( $= 0.002$  pc  $\sim$  nearly 400 AU) was derived leading to a length-to-width ratio of 31. The string's far end is located  $16''.5$  ( $= 0.184$  pc  $\sim 38$  000 AU) from the star.

The morphology of string 2 is very different from that of string 1. In contrast to the nearly straight line image of string 1, string 2 shows a prominent kink (Fig. 2) where the direction of the string changes by  $22^\circ \pm 2^\circ$ . String 2 has a more uniform surface brightness and has a clearer end where the surface brightness drops abruptly.

*String 3* is one of the two strings found in the north-western part of the Homunculus nebula (Fig. 3). We derive a length of  $7''.6$  ( $= 0.085$  pc  $\sim 17$  500 AU). The string is covered in both the WFC and the PC images in its full length, so that the width of the string over its entire observed length can be measured. The width is  $0''.19 = 0.002$  pc ( $\sim 400$  AU) and does not change significantly along the string. This results in a length-to-width ratio of 42. Extrapolating the string back to the star we derive a length of  $17''.0$  ( $= 0.189$  pc  $\sim 39$  000 AU). String 3 is the straightest of all strings and shows only one small wiggle at its outer end. The string's surface brightness is very homogenous, showing nearly no changes in its intensity.

*String 4* lies close to string 3 (Fig. 3) and has similar parameters. Its length amounts to  $9''.3$  ( $= 0.103$  pc  $\sim 21$  400 AU). The width measured on the PC image is  $0''.14$  ( $= 0.002$  pc  $\sim 300$  AU) and is approximately constant along the string. The ratio of length-to-width is 68. Altogether, the string extends  $18''.7$  ( $= 0.208$  pc  $\sim 43$  000 AU) from the star. String 4 bends and wiggles slightly but less frequently than string 1.

*String 5* is much harder to identify due to its low surface brightness. This might also be the reason why it seems less coherent and hard to resolve. It might easily be mistaken as a number of individual filaments. String 5 was measured to be  $5''.2$  long ( $= 0.058$  pc  $\sim 12$  000 AU) and  $0''.14$  ( $= 0.002$  pc  $\sim 300$  AU) wide. This gives a length-to-width ratio of 38. A length

**Fig. 4.** Positions and naming convention of the slits

of  $18''.7$  ( $= 0.208$  pc  $\sim 43$  000 AU) was obtained for the full distance from  $\eta$  Car to the outer end of string 5.

String 5 shows more brightness variations along its extension than the others, giving it a somewhat knotty appearance. The three brightest regions of the string can be identified in Fig. 2. String 5 shows one larger bend, but no small scale wiggles are found.

Note also that at their far ends from the star, strings 1 and 5 become brighter, in contrast to the other strings. In string 1 this brightening looks like two knots.

#### 4. Kinematic analysis

We obtained kinematic data for three of the five strings, using long-slit echelle observations. String 1 was covered in Slits 30S, 32S, 34S and 36S (see Table 2). String 2 was intercepted by Slits 36S and 38S (Table 3), string 5 was found in Slits 36S and 38S (Table 4). The positions of the slits are shown in Fig. 4, the corresponding echellograms in Fig. 5. The spectral axis covers  $80 \text{ \AA}$  and is centred on the H $\alpha$  line at  $6563 \text{ \AA}$ .

In addition to the emission from the Homunculus and its immediate surroundings, the spectra show prominent H $\alpha$  and [N II] 6548 and [N II] 6583 lines which are split by about  $40 \text{ km s}^{-1}$  and which are due to the expansion of the background nebula (Deharveng & Maucherat 1975).

Strings 1, 2, and 5 are marked in Fig. 5 at the [N II] 6583  $\text{\AA}$  line position. All strings show a slope in their respective spectra, indicating a linearly increasing velocity towards larger distances from the star. The radial velocities of the strings are lowest closest to  $\eta$  Car and increase to the maximum velocity at their far ends. Fig. 6 gives the observed radial velocities as functions of the projected distance from the star for the three strings.

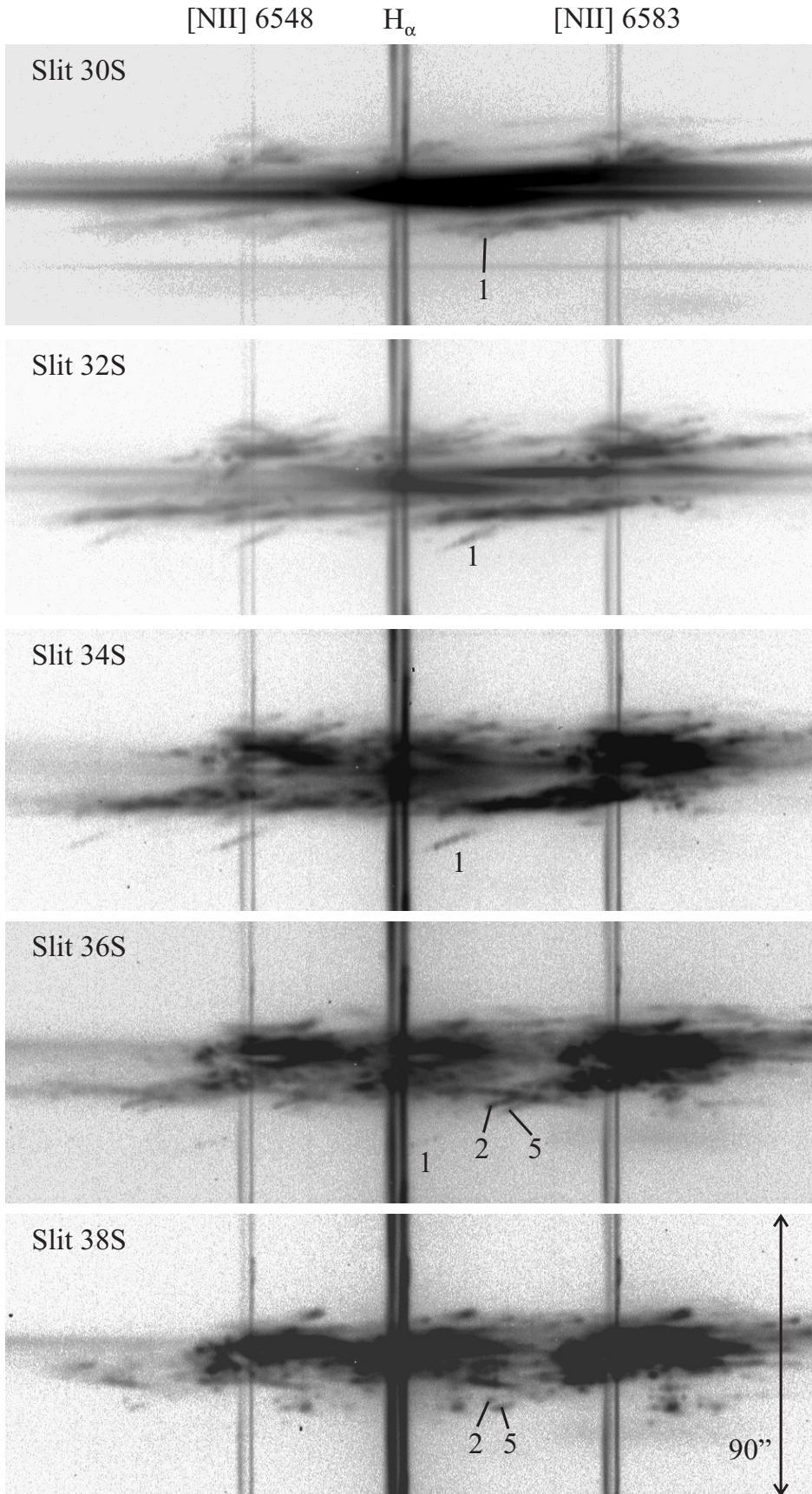


**Fig. 5.** Echellograms at the five slit positions which intercept the strings. Continuous split lines indicate the expansion of the gas in the Keyhole nebula in the vicinity of  $\eta$  Carinae. String 1, 2 and 5 are marked. The spectra were offset by  $2''$  south. Due to the position angle of  $PA=132^\circ$  of the slit the parallel offset is about  $1''.5$ .

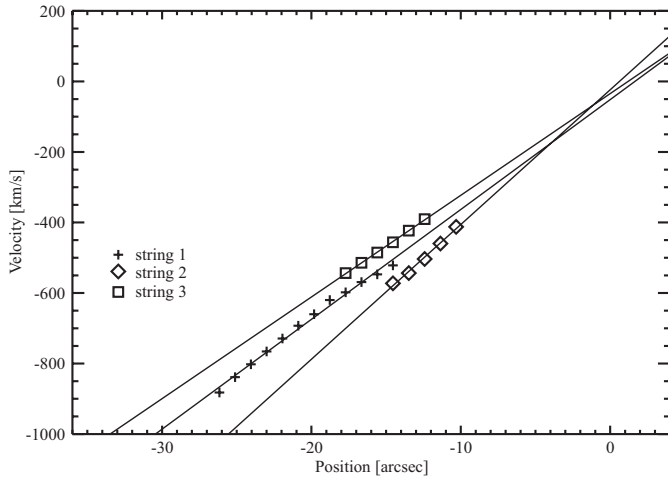


**Fig. 6.** The observed radial velocities as functions of the projected distance from the star for strings 1, 2, and 5.

The velocity increase is very continuous, as seen in Fig. 5. All velocities of strings 1, 2, and 5 are negative, i.e., all strings in the south-eastern part are approaching us, in agreement with the fact that the bipolar lobes of the Homunculus are tilted such that the south-eastern lobe is closer to the observer. Within the uncertainties of our results, the extrapolation backwards leads to a radial velocity of  $0 \text{ km s}^{-1}$  at the position of the star. The main uncertainty comes from the determination of the location of the star relative to the positions of our spectra; we estimate this uncertainty to be about  $1 - 2''$ .

In the following we describe the kinematic parameters of the individual strings:

*String 1* (Table 2): The radial velocities of string 1 range from  $-522 \text{ km s}^{-1}$  at the inner part to  $-996 \text{ km s}^{-1}$  at the far end. The velocity gradient is the same in all spectra, revealing a steady increase of  $31.2 \text{ km s}^{-1}/1'' = 2790 \text{ km s}^{-1} \text{ pc}^{-1}$ . We will comment on this phenomenon in Sect. 5.

Beside the slope, the spectra show that string 1 consists of knot-like substructures (Fig. 5) with distinguishable velocities. The width of the knots in velocity, typically  $22 \text{ km s}^{-1}$ , is larger than the instrumental FWHM of  $14 \text{ km s}^{-1}$  implying the knots are at least marginally resolved in velocity space. Continuous emission connects the substructures and forms the strings. The knotty structures are most prominent in Slits 34S and 36S, they nearly disappear in Slits 32S and 30S.

In addition to the kinematics, the echelle spectra provide us with information about the nitrogen excitation. For string 1 we find a ratio of  $[\text{N II}]\lambda 6583/\text{H}\alpha \sim 3.3 \pm 0.3$  (Table 1). The ratio is constant along the string. It is in the same range as observed in other regions of the nebula around  $\eta$  Car (Meaburn et al. 1987, 1996 [c.f., in particular their Fig. 5])

*String 2* (Table 3): Analogous to string 1 we found a velocity gradient in string 2 reaching from  $-442 \text{ km s}^{-1}$  at the inner to  $-591 \text{ km s}^{-1}$  at the outer end of the string (Fig. 5). This leads to a velocity increase of  $38.2 \text{ km s}^{-1}/1'' = 3420 \text{ km s}^{-1} \text{ pc}^{-1}$ . No knotty substructures were found.  $[\text{N II}]\lambda 6583/\text{H}\alpha$  yields a

**Table 2.** Position and velocities of string 1

slit	position		$v_{\min}$ [ $\text{km s}^{-1}$ ]	$v_{\max}$ [ $\text{km s}^{-1}$ ]
	from [ $''$ ]	to [ $''$ ]		
Slit 30S	-20.1	-14.3	-667	-522
Slit 32S	-25.4	-14.6	-809	-522
Slit 34S	-26.2	-18.0	-853	-631
Slit 36S	-29.4	-23.0	-996	-758

**Table 3.** Position and velocities of string 2

slit	position		$v_{\min}$ [ $\text{km s}^{-1}$ ]	$v_{\max}$ [ $\text{km s}^{-1}$ ]
	from [ $''$ ]	to [ $''$ ]		
Slit 36S	-15.6	-11.1	-584	-442
Slit 38S	-16.4	-13.5	-591	-533

**Table 4.** Position and velocities of string 5

slit	position		$v_{\min}$ [ $\text{km s}^{-1}$ ]	$v_{\max}$ [ $\text{km s}^{-1}$ ]
	from [ $''$ ]	to [ $''$ ]		
Slit 36S	-16.7	-12.4	-529	-383
Slit 38S	-18.0	-15.1	-565	-456

value of  $2.7 \pm 0.3$ , only slightly different from that found for string 1.

*String 5* (Table 4): This string shows the same behaviour as strings 1 and 2, namely a radial velocity increase towards the outer end. Starting at  $-383 \text{ km s}^{-1}$  it reaches  $-565 \text{ km s}^{-1}$  at the tip. This translates into a gradient of  $28.9 \text{ km s}^{-1}/1'' = 2590 \text{ km s}^{-1} \text{ pc}^{-1}$ . The change in velocity is constant. No knotty substructures were detected.

Measuring the line ratio for string 5 was complicated by a large amount of diffuse background emission at the  $\text{H}\alpha$  line (see Figs. 5). We measured a ratio of  $[\text{N II}]\lambda 6583/\text{H}\alpha \simeq 3.0 \pm 0.3$ , taking into account the background contamination.

Based on the assumption that the strings were not accelerated or decelerated considerably since their formation, and that they were formed together with the Homunculus  $\sim 150$  yrs ago, we can determine the inclination  $\phi$  of the strings with respect to the plane of the sky<sup>2</sup> ( $\tan \phi = v_r t s^{-1}$ , where the parameters are defined as follows:  $v_r :=$  radial velocity  $s :=$  projected length and  $t :=$  time since eruption in 1843), and find angles of  $22^\circ$  for string 1,  $27^\circ$  for string 2, and  $20^\circ$  for string 5, respectively. The accuracy of this determination is determined by the positional accuracy of our velocity measurements relative to the star; we estimate the accuracy of the angles to  $\sim \pm 3^\circ$ . This orients the strings roughly in the direction of the major axis of the Homunculus.

For the strings in the north-western part of the Homunculus nebula we could not extract unambiguous kinematic information because the spectra taken at the positions of the strings contain too much diffuse and continuous emission. From our measurements of other features and guided by the assumption

<sup>2</sup> An independent determination of the strings' inclination and expansion age is not possible as we have the velocity and positional informations in directions orthogonal to each other only.

that the strings follow the general tilt of the Homunculus, we would be surprised if strings 3 and 4 do not have positive radial velocities.

## 5. Discussion and conclusions

At the end of core hydrogen burning the most massive stars enter a short ( $\sim 25\,000$  yrs) but violent phase of evolution when they turn into LBVs. This phase is characterized by a high mass loss rate (up to  $10^{-4} M_{\odot}$ , and even more during giant eruptions) and intermittent *giant eruptions*. During these eruptions the star's visual luminosity increases by several magnitudes. The mechanism causing this behaviour is still far from understood. High mass loss and giant eruptions lead to the formation of the nebulae around the LBVs. García-Segura et al. (1996) and Dwarkadas and Balick (1998) showed in a hydrodynamic model that the interaction of an older slow and a younger fast wind in the LBV phase may give rise to the structure of the LBVN.

One finds LBVNs in very different shapes and sizes. A comprehensive compilation of nebulae around LBVs known as yet may be found in Nota et al. (1995). Already ground-based images revealed that most of the LBVNs have small-scale substructures like knots and arcs. These features can be seen in detail in recent HST images, e.g. of AG Car, HR Car. In particular the Homunculus nebula around  $\eta$  Car contains a large variety of substructures and individual knots (e.g., Walborn 1976). Beside the knotty structure of the central bipolar lobes (diameter of each lobe:  $\sim 0.1$  pc) numerous filaments exceed the size of the central nebula and can be found at distances up to  $30''$  or  $\sim 0.3$  pc from the star (see Fig. 1).

When analyzing these structures around  $\eta$  Car, we find that the strings show amazing and unexpected characteristics. They are *extremely narrow* with *very high length-to-width ratios*, generally *very straight*, and they follow a *perfectly linear velocity increase* towards increasing distances from the star. Back-extrapolation of this linear dependency to the position of the star is consistent with a vanishing radial velocity there, i.e., we have a projected distance-radial velocity law of the *Hubble type*.

### 5.1. The nature of the strings

The physical nature of the strings is far from understood yet. They may or may not be a single physical entity. One may think of a coherent structure, similar to a water jet, for instance. However, one may equally well envisage a train of many individual knots or bullets following the same path. One also cannot rule out the possibility that they are trails or wakes following an object at the strings' far ends, or even projection effects of the walls of, for instance, much wider funnels.

Currently, one can only speculate about the reasons for

- the *straightness* of the strings: This may point to an origin of the strings at a much smaller distance from the star than their current location, for instance at or close to the star's surface. Then even Keplerian azimuthal velocity and the accompanying angular momentum would result in a negligible

azimuthal velocity at their current location as long as they do not gain considerable amounts of angular momentum during their evolution, which is certainly a reasonable assumption. Slight deviations from the straight expansion may be due to deflections caused by interaction with the local ambient medium;

- the *narrowness and collimation* of the strings: Most likely, it is due to their highly supersonic expansion velocities. If – at best – the lateral expansion is at thermal speeds, then this corresponds to “opening angles” of the strings of  $1^{\circ}$  or less, i.e., far less than can be detected in the available body of imaging data. This seems to indicate that the narrowness itself was defined in the origin of the strings.
- the *Hubble type velocity law* of the strings: While a geometric projection effect is extremely unlikely, one may think of several possible other mechanisms, or combinations of them.
  - *Stellar winds*: For stellar winds, for a certain radial range in the vicinity of the star at several, but not many stellar radii, a linear velocity profile is a good approximation. In our case, however, the geometrical dimension of the strings is very much larger than the stellar radius, making such an interpretation again very unlikely. However, if the working surface of the acceleration process were much larger than the star itself and no longer small compared to the radial dimensions of the string, it could give rise to such a linear profile.
  - *Stellar explosions*: In stellar explosions – rather than winds – a linear velocity profile is a good approximation for the larger radii, close to the head of the explosion (Tscharnuter & Winkler 1979). Given the highly supersonic velocities of the strings, such a stellar explosion may be a viable model for the velocity evolution of the strings.
  - *Primordial velocity spectrum*: At their formation the strings were ejected within a time scale that is short compared to the time scale of the evolution since then, and this ejection happened with a certain distribution of velocities.

In any case, it is noteworthy that such a linear expansion law is also observed for the proper motion of the main structures of the Homunculus (Currie et al. 1996).

In summary, one has to conclude that the linear velocity law of the strings is far from being really understood. However, the orientation of the strings - assuming a certain epoch of formation - points towards a close relation to the event that also created the Homunculus, as do the results of the Hubble-type law.

### 5.2. Are the strings unique?

Even though many of the LBVN show small scale structures and knots, no strings were found in other LBVNs. In particular for AG Car and HR Car, on HST images one should be able to detect narrow strings of the type seen around  $\eta$  Car, but none were found. In the light of the ongoing discussion about

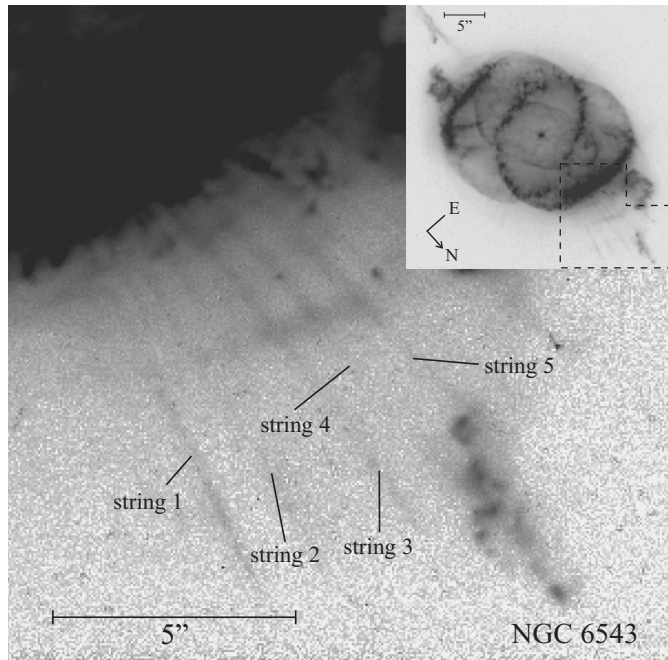


**Fig. 7.** The planetray nebula NGC 6543 observed with the HST F658N filter. In the insert the whole nebula with the central PN star is shown while the large image shows the northern section of the PN nebula with 5 string-like objects similar to what we identified in  $\eta$  Car.

**Table 5.** Parameters of strings like structures in NGC 6543, for the width the minimum and maximum values are listed

string	length [ $10^{-3}$ pc]	width [ $10^{-3}$ pc]	length-to-width
1	39	0.8–1.3	30–50
2	43	0.5–1.3	33–82
3	39	0.5–1.3	30–74
4	43	0.5–1.5	10–30
5	35	1.5–2.1	17–22

morphological and physical similarities and relations between LBVN and planetary nebulae (see, e.g., Frank et al. 1998, Frank 1998, Currie & Dowling 1999), it is of interest to look into the question whether the strings and their properties are unique to LBVNs.

We re-analyzed the HST images of NGC 6543 from the CAD archive ([N II] F658N filter) and found at least 5 (possibly 2 more) features (Fig. 7) that resemble our strings very much (see also in Harrington & Borkowki 1994, 1995). The PC again allowed us to determine the width of the strings between 2–8 pixel. Assuming a distance to NGC 6543 of 1170 pc (Castor et al. 1981) we found that the string lengths are  $35 \cdot 10^{-3}$  to  $43 \cdot 10^{-3}$  pc while they are  $0.5 \cdot 10^{-3}$  to  $2.1 \cdot 10^{-3}$  pc wide (Table 5). Their length-to-width ratios range from 22 to 82. Comparing these string-like structures with the strings in  $\eta$  Car we conclude that they show approximately the same morphology. The linear sizes are comparable. A comparison between these PN-strings and the ones in LBVs, which we discussed in the present paper,

will be of utmost importance as it has the potential of yielding insight into the differences and into the similarities in the formation processes of nebular structures around evolved high (LBV) and low (PN) mass stars.

**Acknowledgements.** The data reduction and analysis was in part carried out on a workstation provided by the *Alfried Krupp von Bohlen und Halbach Stiftung*. This support is gratefully acknowledged. We thank D.J. Bomans, Bochum, for many stimulating discussions of the subject of this paper, and the referee for helpful comments. Guest User, Canadian Astronomy Data Centre, operated by the Herzberg Institute of Astrophysics, National Research Council of Canada.

## References

- Castor J.I., Lutz J.H., Seaton M.J., 1981, MNRAS 194, 547  
 Currie D.G., Dowling D.M., 1999, ASP Conf.Ser. 179 (in press)  
 Currie D.G., Dowling D.M., Shaya E.J., et al. 1996, AJ 112, 1115  
 Daminieli A., 1996, ApJ 460, L49  
 Daminieli A., Conti P.S., Lopes D.F., 1997, New Astronomy 2, 107  
 Davidson K., 1997, New Astronomy 2, 387  
 Davidson K., Humphreys R.M., 1997, ARA&A 35, 1  
 Deharveng L., Maucherat M., 1975, A&A 41, 27  
 Duschl W.J., Hofmann K.-H., Rigaut F., Weigelt G., 1995, RevMexAA SdC 2, 41  
 Dwarkadas V.V., Balick B., 1998, AJ 116, 829  
 Frank A., 1998 astro-ph/9805275  
 Frank A., Ryu D., Davidson K., 1998, ApJ 500, 291  
 García-Segura G., Mac Low M.-M., Langer N., 1996, A&A 305, 229  
 Gaviola E., 1946, Revista Astronomica 18, 252  
 Gaviola E., 1950, ApJ 111, 408  
 Harrington J.P., Borkowki K.J., 1994, BAAS 26, 1469  
 Harrington J.P., Borkowki K.J., 1995, Press Release STScI-PRC95-01  
 Herschel J.F.W., 1847, Results of Astronomical Observations Made During the Years 1834-1888 at the Cape of Good Hope, London, 32  
 Hillier D.J., Allen D.A., 1992, A&A 262, 153  
 Humphreys R.M., 1978, ApJS 38, 309  
 Humphreys R.M., 1979, ApJS 39, 389  
 Humphreys R.M., Davidson K., 1979, ApJ 232, 409  
 Humphreys R.M., Davidson K., 1994, PASP 106, 1025  
 Innes R.T.A., 1903, Cape Ann., 9, 75B  
 Langer N., Hamann W.-R., Lennon M. et al., 1994, A&A 290, 819  
 Meaburn J., Wolstencroft R.D., Walsh J.R., 1987, A&A 181, 333  
 Meaburn J., Walsh J.R., Wolstencroft R.D., 1993, A&A 268, 283  
 Meaburn J., Boumis P., Walsh J.R. et al., 1996, MNRAS 282, 1313  
 Morse J.A., Davidson K., Bally J. et al., 1998, AJ 116, 2443  
 Nota A., Livio M., Clampin M., 1995, ApJ 448, 788  
 Smith N., Gehrz R.D., 1998, AJ 116, 823  
 Thackeray A.D., 1949, Observatory 69, 31  
 Thackeray A.D., 1950, MNRAS 110, 524  
 Thé P.S., Bakker R., Antalova A., 1980, A&AS 41, 93  
 Tscharnuter W.M., Winkler K.-H., 1979, Comp.Phys.Comm. 18, 171  
 van Genderen A. M., Thé P.S., 1984, Space Sci. Rev. 39, 317  
 Viotti R., 1995, RevMexAA SdC 2, 10  
 Walborn N.R., 1976, ApJ 204, L17  
 Walborn N.R., 1995, RevMexAA SdC 2, 51  
 Walborn N.R., Blanco B.M., Thackeray A.D., 1978, ApJ 219, 498  
 Walborn N.R., Blanco B.M., 1988, PASP 100, 797